Quantum-Chemistry-Based Force Field for Simulations of Dimethylnitramine

ARTICLE *in* THE JOURNAL OF PHYSICAL CHEMISTRY B · JANUARY 1999

Impact Factor: 3.3 · DOI: 10.1021/jp9834006

4 AUTHORS, INCLUDING:

Dmitry Bedrov
University of Utah
164 PUBLICATIONS **3,151** CITATIONS

SEE PROFILE

A Quantum Chemistry Based Force Field for Simulations of Dimethylnitramine

Rishikesh K. Bharadwaj and Grant D. Smith*

Department of Materials Science and Engineering and
Department of Chemical and Fuels Engineering
University of Utah
Salt Lake City, UT 84112

Abstract

The molecular geometries and conformational energies of nitramide and dimethylnitramine (DMNA), determined from high level quantum chemistry calculations, have been used in parametrization of a classical potential function suitable for simulations of DMNA. A thorough investigation of basis set size and electron correlation effects on the geometry and conformational energies of nitramide, for which accurate experimental data exist, has allowed us to establish the level of theory required to obtain accurate geometries and energies for nitramine compounds. These investigations revealed the importance of electron correlation for both the geometries and relative conformational energies in nitramines. The quantum chemistry based force field for DMNA was validated by comparing gas and liquid-phase properties obtained from molecular dynamics simulations with available experimental data. The gas-phase radial distribution function obtained from simulation is in good agreement with that obtained from electron diffraction experiments, and is consistent with a C_s ground-state geometry for DMNA as predicted by quantum chemistry. The pressure-volume-temperature properties and solubility parameters for the bulk liquid are in very good agreement with available experimental measurements. The correlation time and activation energy associated with molecular reorientation is found to be in good agreement with NMR measurements.

* To whom correspondence should be addressed.

I. Introduction

Nitramines such as RDX (hexahydro-1,3,5-trinitro-1,3,5-triazine), HMX (octahydro-1,3,5,7-tetranitro-1,3,5,7-tetraazocine), and DMNA (dimethylnitramine), are important high-energy materials. Used in conjunction with polymeric binders, these materials form the basis of many solid propellants and high explosives. Understanding the thermophysical, mechanical, aging and chemical behavior of these systems is vital for efficient stewardship of nuclear stockpiles. In the context of limitations imposed by the comprehensive nuclear test ban treaty, it has become imperative that the capability to accurately simulate mechanical, thermodynamic, and chemical behavior of these materials be developed.

DMNA is a clear choice as a model compound to lead to a better understanding of the more complex but chemically similar explosives such as RDX and HMX. In the present study, DMNA has been chosen as the building block in the process of developing force field parameters for performing classical molecular dynamics (MD) simulations of RDX and HMX. Our experience has shown that atomistic MD simulations can accurately reproduce thermophysical properties of condensed phases of small organics provided that the geometries as well as intramolecular and intermolecular interactions, obtainable from high-level quantum chemistry, are well described by the potential energy functions, or force field, employed in the simulations.[1] These quantum chemistry based force fields are in turn transferable to larger oligomers or even polymers.[2]

Previous studies of RDX[3] and HMX[4] have shown that intermolecular interactions in nitramines can be accurately described with simple two-body dispersion/repulsion and coulomb (partial atomic charge) terms. This work, which involved modeling of the crystalline phases of RDX and HMX, treated the molecules as rigid, and hence did not address conformational and inversion energies in the molecules. Our experience with flexible molecules indicates that it is critical that the flexibility of the molecule be

accurately described in order to accurately reproduce thermophysical properties, particularly transport properties, of amorphous phases. Ab initio quantum chemistry has proven to be an invaluable source of geometric and energetic data necessary to develop intramolecular potential energy functions for conformationally flexible molecules.

In this study, we describe our ab initio studies of the geometry and flexibility of nitramide and DMNA. Nitramines undergo inversion about the amine nitrogen, as illustrated in Figure 1(a) and 1(b) for nitramide. They also have conformational flexibility for rotation of the nitro group about the N-N bond, also illustrated in Figure 1(a). Experimental data are available for the inversion energy in nitramide, making this a useful model for determining the level of theory needed in the quantum chemistry studies to reproduce these energies in nitramines. The larger (RDX and HMX) nitramines also demonstrate conformational flexibility due to rotation about the C-N—C-N bonds. We will consider the force field development and quantum chemistry of HMX in an upcoming publication. Based upon our quantum chemistry studies of nitramide and DMNA, we have parametrized an atomistic force field for DMNA that accurately reproduces the ground state and inversion saddle point geometries, as well as the inversion energy, methyl group rotational energy and nitro group rotational energy. In this paper, we compare predictions from MD simulations of gas and liquid-phase DMNA with available experimental data. In an upcoming paper we will report on the transport and structural properties of the liquid, and on the structure and elastic constants of crystalline DMNA.

II. Quantum Chemistry Studies

Previous work. Ritchie[5] investigated the geometry, inversion energy, and nitro group rotational energy in nitramide for 3-21G and 6-31G* basis sets at both the SCF and MP2 levels. He found that the polarization functions in the larger basis set were necessary to

correctly predict the nonplanarity of the ground-state structure, as illustrated in Figure 1(a). Additionally, he found that the inversion energy and nitro group rotation energy depend strongly upon electron correlation. Sumpter and Thompson[6], Politzer et al.[7], and Kohno et al.[8] performed ab initio studies of DMNA using 6-31G or smaller basis sets, and found the planar C_{2v} structure to be the ground state. Roszack[9] using MC-SCF calculations on DMNA reported a similar result. Khaikin et al.[10] performed DMNA geometry optimizations at the SCF/6-31G* and MP2/6-31G* levels, and found that the nonplanar C_s structure to be the ground state, with the planar C_{2V} structure corresponding to an inversion saddle point, analogous to earlier studies for nitramide[5]. They obtained an inversion energy of 1.2 kcal/mol and a nitro group rotational energy barrier of 9.9 kcal/mol at the MP2 level. Harris and Lammertsma[11] performed density functional calculations at the B3LYP/6-31G* level and found the ground state geometry of DMNA to be of C_s symmetry with significant pyramidal character associated with the amine nitrogen.

Level of Theory. Quantum chemistry calculations were performed using Gaussian 94.[12] We have systematically investigated the influence of basis set, electron correlation, and geometry optimization on the inversion barrier in nitramide, where an experimental estimate of 2.7 kcal/mol[13] is available. Results of this investigation are given in Table 1.

The effect of electron correlation on the ground state and saddle point geometries of nitramide was also investigated. The ground state nitramide geometries determined at the SCF and MP2 levels with 6-31G*, 6-311G* and 6-311G** basis sets are compared in Table 2. Also shown are gas-phase geometries determined from microwave measurements[14] and gas-phase electron diffraction[15]. The MP2 geometries differ significantly from the SCF geometries, particularly for the O-N and N-N bond lengths. The MP2 geometries are in better agreement with experimental estimates. MP2 inversion energies obtained using SCF geometries are 0.2 to 0.4 kcal/mole lower than those found using MP2 geometries for the 6-31G*, 6-311G* and 6-311G** basis sets. It appears that inclusion of correlation effects in both geometry optimizations and in energy calculations is required in order to obtain accurate values for the inversion barriers in nitramides. The geometry shows only a very weak dependence on basis set. Therefore, we performed larger basis set calculations for nitramide using the MP2/6-311G** geometries.

The influence of augmentations of the basis set over 6-311G** on the inversion barrier energy was systematically investigated at the MP2 level using the MP2/6-311G** geometries. Compared to the MP2/6-311G** value, additional diffuse functions on the heavy atoms (6-311+G**) results in a 0.3 kcal/mol decrease in the inversion energy while additional diffuse functions on the hydrogen atoms (6-311++G**) results in little additional change. Additional polarization functions on the heavy atoms (6-311G(2d,p)) results in a dramatic decrease in the inversion energy. The inversion energy further decreases when f functions are considered (6-311G(2df,p)). Additional polarization functions on the heavy atoms (6-311G(3df,p) and 6-311G(3d2f,p)) make almost no difference in the inversion energy. Compared to the 6-311G(2df,p) energies, additional polarization function for the hydrogen atoms (6-311G(2df,2p)) substantially increases the inversion barrier. Additional p functions for hydrogen atoms makes almost no difference in the inversion barrier, as can be seen by comparing the 6-311+G(2df,2p) and 6-

311+G(2df,3p) energies. We conclude that addition of basis functions beyond 6-311+G(2df,2p) can be expected to make little difference to the inversion energy.

Using the 6-311+G(2df,2p) basis set, we again examined the inversion energy as a function of electron correlation treatment. As was found for the smaller 6-31G* basis set, the MP2 level calculations tend to underestimate the inversion barrier compared with the CCSD(T) energies. As the latter are prohibitively expensive for larger molecules, we determined to carry out calculations on DMNA at the MP2/6-311G(2df,2p)//MP2/6-311G** level. This level of calculation yields an inversion energy of 2.57 kcal/mol, in excellent agreement with the CCSD(T)/6-311+(2df,2p) value of 2.55 kcal/mol. The lower inversion barrier predicted at the MP2 level is approximately accounted for by neglect of the additional diffuse functions for the heavy atoms in the smaller basis set, which also lowers the inversion barrier. The ground-state dipole moment was found to be 3.403 D at the MP2/6-311G(2df,2p)//MP2/6-311G** level which is in good agreement with the experimental gas-phase values of 3.57[14] and 3.75 D [16].

III. Quantum Chemistry Results for Dimethylnitramine

Geometry. The ground state (C_s) and transition state for inversion (C_{2V}), and the transition state for rotation (C_s) geometries of DMNA, illustrated in Figure 1(d), (e) and (f) respectively, were determined at the MP2/6-311G** level and are given in Table 3. Also shown are experimental values from electron diffraction[17] and x-ray diffraction studies[18]. As with nitramide, the importance of including electron correlation in the geometry optimization of DMNA is manifest. The predicted ground state of DMNA is of C_s symmetry with the amine nitrogen showing significant pyramidal character. This is in fact true of all levels (SCF and MP2) of calculation, except when 6-31G and smaller basis sets are employed. The angle between the N-N bond and the C-N-C plane is found to be 41º at the MP2 and 31º at the SCF levels. These results differ considerably from the

experimental gas phase geometry, which has been predicted to be of C_{2v} (planar) symmetry based upon electron diffraction measurements.[17] This apparent discrepancy is further addressed below. In the crystalline phase DMNA adopts a planar conformation as given by x-ray diffraction.[18] However, pyramidalization at the amine nitrogen is found in the low temperature crystalline form of DMNA[19] to an extent of about 10º. It can be concluded that the preference for planar or pyramidal nature is sufficiently weak that intermolecular interactions in condensed phases (crystalline) are capable of altering the geometry from that which is observed in the gas phase. The preferred geometry in the liquid phase is unknown from experiment, but is predicted to be pyramidal from our simulations (see below).

Energies. The inversion energy in DMNA, determined at the MP2/6-311G(2df,2p)//MP2/6-311G** level was found to be 0.89 kcal/mol. This is significantly lower than the 2.57 kcal/mol found in nitramide at the same level. The barrier for rotation of the methyl group was found to be 1.63 kcal/mol at the MP2/6-311G(2df,2p)//MP2/6-311G** level. The conformational energy as a function of nitro group dihedral angle O-N—N-O (see Figure 1(c)) at this level of theory is shown in Figure 2. The nitro group dihedral is –159.2° at the ground state and –59.5° at the rotational barrier, with both states possessing C_s symmetry as denoted in Figure 1(d) and (f) respectively. A barrier energy of 10.58 kcal/mol is obtained at the MP2/6-311G(2df,2p)//MP2/6-311G** level in good agreement with experimental estimate of >9 kcal/mol.[20] The rotational barrier configuration with C_{2V} symmetry (with planar CNCN configuration) leads to a barrier that is approximately twice the experimental estimate.

Zero-point, thermal vibrational and rotational contributions. The contributions of zero-point energy, thermal vibrational energy and entropy and thermal rotational entropy to the relative free energies of the nitramide and DMNA inversion barrier configurations relative the respective ground states were investigated using harmonic

frequencies obtained at the MP2/6-311G** level. At 298 K, these contributions lower the free energy of the C_s saddle point relative to the C_{2v} ground state by 0.97 and 0.57 kcal/mol at the MP2/6-311G** level for nitramide and DMNA, respectively. The inversion barrier at the same level is found to be 3.43 kcal/mol for nitramide, and hence is lowered to 2.46 kcal/mol after correction. This value is very close to the value of 2.57 kcal/mol predicted at the MP2/6-311G(2df,2p) level for nitramine, which is in very good agreement with the experimental result of 2.7 kcal/mol. Applying the MP2/6-311G** level corrections to the MP2/6-311G(2df,2p) energy would result in a lower barrier and hence a large deviation from the experimental value. For DMNA, the inversion barrier is reduced from 1.79 to 1.22 kcal/mol after correction. The value at the MP2/6-311G(2df,2p) level is found to be 0.89 kcal/mol which is close to the corrected value from the MP2/6-311G** level. Therefore, the MP2/6-311(2df,2p) values were used without correcting for zero-point, thermal vibrational and rotational effects. Alternatively, using MP2/6-311G** energies with correction appears to yield similar results.

Finally, it can be noted the MP2/6-311G(2df,2p)//MP2/6-311G** level of theory yields not only an inversion barrier for nitramide in good agreement with experiment, but also inversion barriers for ammonia (6.14 kcal/mol vs. 5.8 kcal/mol from experiment[21]) and methylamine (5.8 kcal/mol vs. 4.8 kcal/mol from experiment[22]).

IV. Force Field Parametrization

A potential energy function of the form

$$U = U^{\text{stretch}} + U^{\text{bend}} + U^{\text{torsion}} + U^{\text{improper torsion}} + U^{\text{dispersion}} + U^{\text{coulomb}} \quad (1)$$

was parametrized to reproduce the ground-state and inversion geometries, inversion energy, ground-state dipole moment, methyl group rotation and nitro group rotation in DMNA.

Valence Parameters. The stretching force constants were obtained from normal-mode analysis of DMNA at the SCF/6-311G** level for the ground-state geometry. The force constants were scaled by 0.80 to account for deficiencies in the SCF force constants and anharmonic effects. The values are given in Table 4. The equilibrium bond lengths were determined so as to match the MP2/6-311G** ground state geometry, with a slight increase to account for anharmonic effects. A comparison of ab initio and force field geometries for DMNA in the ground state and at the inversion barrier is shown in Table 3.

The bending force constants are such as to be consistent with the internal coordinate force constants obtained at the SCF/6-311G** level, except for the N-C-H and H-C-H, where constants were obtained from the MOLBD3[23] database. The equilibrium angle parameters were adjusted to give the best representation of the ground state and inversion barrier geometries for DMNA, as compared in Table 2, and to reproduce the inversion energy in DMNA. The force field yields a value of 0.81 for the inversion barrier, in good agreement with the quantum chemistry value of 0.89 kcal/mol.

Torsional Parameters. The torsional parameters were adjusted to give the best representation of the methyl and nitro group rotation. The three-fold H-C-N-N function allows for exact reproduction of the methyl group rotational barrier of 1.63 kcal/mol. The ability of the force field to represent the nitro group rotation is illustrated in Figure 2. Emphasis was placed on accurate representation of the conformational energy in the vicinity of the minima, which tend to be highly populated due to the very high barrier (11.50 kcal/mol vs. 10.58 kcal/mol from quantum chemistry). In addition, an improper torsion, or out-of-plane bending, function for the nitro group was parametrized to reproduce the distortion energy of the nitro group obtained from ab initio studies.

Nonbonded Parameters. The exp-6 repulsion/dispersion parameters were taken from previous work.[24,25] The parameters for carbon, hydrogen, and oxygen were taken

from Sorensen et al.[24] The nonbonded parameters for nitrogen were determined so as to accurately reproduce the gas-phase second virial coefficient of trimethylamine as a function of temperature.[25] In calibrating the N-N potential, the potential parameters for C, H, and O were taken from previous work.[24] Standard combining rules were employed in describing interactions between disparate atom pairs except for C-H. The partial atomic charges were obtained by fitting to the electrostatic potential at a grid of points produced from the MP2/6-311G(2df,2p) wave functions. In the fitting, the methyl hydrogen atoms were constrained to have equal charges, and the grid (30,000 points) extended from 1.8 Å (for H, N, O) and 2.5 Å (for C) to 3.5 Å for the atom centers. The dipole moment from the partial atomic charges is 3.95 D, in good agreement with the quantum chemistry (MP2/6-311G(2df,2p)//MP2/6-311G**) value of 3.96 D for the C_s ground-state molecule. The experimental gas phase dipole moment is found to be 4.61 D. The dipole moment of the C_{2V} molecule was found to be 4.54 D from quantum chemistry.

V. Gas Phase Simulation

Structure. As pointed out above, there is a contradiction between the ground-state geometry of DMNA gleaned from gas-phase electron diffraction measurements and that predicted by quantum chemistry (and hence by the force field). In order to help resolve this discrepancy and to validate the force field parameters, Brownian dynamics (BD) simulations of a gas-phase DMNA system consisting of 108 molecules were performed using the quantum chemistry based force field without intermolecular interactions. For these simulations, the methodology described by van Gunsteren and Berendsen[26] was employed. Equilibration of 100 ps was followed by a sampling trajectory of 500 ps. A frictional coefficient of 1.33 $(10)^{-4}$ fs^{-1} was used in the simulation.

The radial distribution function *g(r)* has been computed from BD trajectories at 350 K using the following relationship,[27]

$$g(r) = \frac{p}{2} \sum_{i} \sum_{\substack{j \\ j \neq i}} \left(\frac{z_i z_j}{\sum_i z_i^2 + z_i} \right) \frac{p(r)}{r}, \qquad (2)$$

where, z_i is the atomic number of species *i* and *p(r)* is the probability of finding an atom pair at a radial distance *r*. The radial distribution functions are shown in Figure 3, where the results from the simulation are compared with the experimental[17] *g(r)* at 343 K. All the significant peaks have been indexed according to their source of origin. The disparity in peak heights for the distances corresponding to the bond lengths is due to the neglect of zero-point vibrational effects in the simulation. Notwithstanding this feature, it is seen that the agreement is excellent both in terms of peak heights and positions for the three center (bending) and higher (torsions and further removed) interactions. An important implication of this agreement is that *g(r)* is insensitive to the presence or absence of pyramidal character at the amine nitrogen. The simulation results correspond to a puckered molecule, and it is seen that the distance between the C and O atoms from simulation is nearly identical to that given experimentally. This insensitivity was further confirmed by performing gas-phase simulations using a potential function with a much lower inversion barrier. These yielded a *g(r)* essentially indistinguishable from that shown in Figure 3. Hence, we believe that the ground-state geometry of gas-phase DMNA cannot be unambiguously assigned based upon the electron diffraction measurements. Based upon quantum chemistry and gas-phase BD simulations, which yield a *g(r)* consistent with experiment, we conclude that the ground-state geometry of DMNA in the gas-phase is of C_s symmetry.

Free Energy Barrier to Inversion. The effective inversion potential $V_{eff}(d)$ based on the probability distribution of the inversion angle (defined as the angle between the plane containing the C-N-C atoms and the N-N bond) was determined from the gas-phase BD simulation populations at 350 K using the relationship

$$V_{eff}(d) = -KT \ln P(d) \quad (3)$$

where K is the Boltzmann constant, T is temperature, and $P(d)$ is the probability of finding a molecule with inversion angle of d relative to that for finding it in the ground state. The effective potential at 350 K is shown in Figure 4 along with quantum chemistry energies (relative to the ground state) for several values of d. The agreement between the simulation and the quantum chemistry is very good considering that only the quantum chemistry energy at the barrier (0º) and the ground state and inversion barrier geometries were considered in parametrizing the force field.

VI. Liquid Phase Simulation

Simulation Details. Simulations of liquid DMNA were performed in order to validate the force field through comparison of PVT (pressure-volume-temperature) properties with experiment. The system comprised of 108 DMNA molecules was run under NPT (constant pressure, temperature and particle number) and NVT (constant volume, temperature and particle number) conditions using extended system dynamics.[28] Explicit reversible integrators were used to solve the equations of motion.[29] The frequency of oscillation for the thermostat and barostat was chosen to be 5 ps^{-1}. Long range corrections to the electrostatic energy and force were calculated using the Ewald summation technique. The bond stretching force constants were attenuated by a factor of four in order to increase the time step. A time step of 1 fs was used.

P-V-T Properties. The specific volumes were monitored over a period of 200 ps as a function of temperature. Specific volumes for this system typically achieved equilibrium values over a time scale of 50 ps. The time averaged specific volumes are plotted versus temperature in Figure 5(a). The agreement between the experiment[30] and simulation is good (simulation being 1.3% higher) at 350 K. The coefficient of thermal expansion in

the temperature range 350-400 K is found to be 7.9 $(10)^{-4}$ K^{-1}. The P-V isotherm at 350 K is shown in Figure 5(b). The isothermal compressibility is found to be 5.33 $(10)^{-5}$ atm^{-1} over 0-750 atm.

Solubility Parameter. The intermolecular portion of the nonbonded and electrostatic energy was taken to be the cohesive energy. The solubility parameter (d) is given by the square root of the cohesive energy density. The temperature dependence of the solubility parameter derived from simulation is shown in Figure 6. Also shown for comparison is the value of d for the same compound at 298 K from experiment[31]. Extrapolation of the MD data, via a second order polynomial fit, to lower temperatures shows excellent agreement with the experimental result. This agreement further reinforces the fact that the force field is correctly reproducing the intermolecular packing energetics of DMNA.

Inversion rate. In order to investigate the effect of intermolecular packing on the inversion barrier, the effective potential from population sampling of the liquid was determined using eq. 3, and the rate to inversion ($C_s \leftrightarrow C_{2v}$) in the liquid was analyzed in terms of the number of barrier crossings. For the latter, the out of plane angle (angle between the C-N-C plane and N-N bond) was monitored during the simulations. A transition was determined to have occurred when the angle underwent a change in its value from one side of the barrier, crossed the barrier (0°), and assumed a value greater than the position of the minimum (±41°) on the other side. The effective potential as obtained from eq. 3 for the liquid phase at 350 K, is shown in Figure 4. Values are nearly identical to those obtained in the gas phase. The transition rate was computed at several temperatures, and shown in an activation map in Figure 7. The transition rate follows Arrhenius behavior with an activation energy of 0.81 kcal/mol. It is thereby concluded that the bulk packing has very little effect on the energetics of the inversion mode in liquid DMNA.

Orientational Relaxation. Molecular reorientational dynamics were studied by computing the first and second order orientational autocorrelation functions (OACF) given by

$$P_1(t) = \langle m_i(0).m_i(t) \rangle = \langle \cos q(t) \rangle, \quad (3)$$

$$P_2(t) = \tfrac{1}{2} \langle 3\cos^2 q(t) - 1 \rangle, \quad (4)$$

where $m_i(0)$ and $m_i(t)$ are the unit vectors defining the orientation of molecule i, and q is the angle between the two vectors separated by time t. In this case, the unit vector considered was taken to be along the N-N bond, and the relaxation of this vector was studied at different temperatures as a function of time.

The resulting autocorrelation functions are displayed in Figure 8. The P_1 and P_2 OACF have been fit with the Kohlrausch-Williams-Watts stretched exponential of the form

$$F(t) = \exp\left[-(t/t_{kww})^b\right], \quad (5)$$

where t_{kww} is the relaxation time associated with the decay and b is the width parameter. The stretched exponential equation fits both P_1 and P_2 autocorrelation functions remarkably well. The t_{kww} values from the fit to P_1 have been plotted as a function of temperature in Figure 9. The temperature dependence is Arrhenius in nature with an attendant activation energy of 2.76 kcal/mol.

The correlation time and activation energy associated with molecular reorientation in DMNA has been investigated using ^{14}N NMR measurements of the nuclear quadrupolar relaxation of the nitrogen in the nitro group.[20] This relaxation is related to the molecular P_2 OACF. In the extreme-narrowing regime, the experimentally measured quadrupolar relaxation time is simply related to the orientation correlation time. Taking the N-N unit

vector, represented by eq. 5, as representative of the molecular orientation, the correlation time, t_c is given by

$$t_c = \int_0^\infty P_2(t)dt = \int_0^\infty F(t)dt = \frac{t_{kww}}{b}\Gamma(1/b). \qquad (6)$$

The temperature dependence of t_{kww} and t_c is shown in Figure 9. The activation energies are also shown. The results are summarized in Table 5 along with the experimental values in two solvents at 298 K. The activation energies and correlation time obtained from our neat-liquid simulation are quite similar to those obtained experimentally for DMNA in solution. Subsequently, we can anticipate high diffusion coefficients and low viscosities for DMNA liquid.

VII. Conclusions

The importance of incorporating electron correlation in performing geometry optimizations and in determining relative conformational energies in nitramines has been demonstrated through a systematic analysis of nitramide and DMNA. Very good agreement with experiment for the molecular geometry and inversion energy of nitramide was obtained by performing geometry optimization at the MP2/6-311G** and subsequent single point energy calculations at the MP2/6-311G(2df,2p) level. Force field parameters were derived for DMNA based upon quantum chemistry calculations performed at this level for use in classical molecular dynamics simulations. The quantum chemistry calculations establish ground state of DMNA to be of C_s symmetry (pyramidal) in contrast to previous analysis of gas-phase electron diffraction result that predicted a C_{2v} (planar) molecule. The structure of the DMNA in the gas phase as predicted by Brownian dynamics simulation using the quantum chemistry based force field is in good agreement

with experimental electron diffraction results, lending further credibility to the pyramidal C_s molecule being the ground state configuration.

Liquid-phase properties such as P-V-T behavior and the solubility parameter as obtained from MD simulations using the quantum chemistry based force field show very good agreement with experimental results. The barrier to inversion in the liquid state is found to be similar to that in the gas phase, indicating the absence of any condensed phase effects on the energetics of the inversion mode in the liquid. The correlation time and activation energy obtained for the relaxation of the second order OACF are in very good agreement with NMR measurements of quadrupolar relaxation of DMNA in solution.

Acknowledgment

This research is funded in part by the University of Utah Center for the Simulation of Accidental Fires and Explosions (C-SAFE), funded by the Department of Energy, Lawrence Livermore National Laboratory, under subcontract B341493. The authors gratefully acknowledge the assistance of Professor R.H. Boyd in this endeavor.

Table 1

Influence of Basis Set and Electron Correlation on the Inversion Barrier for Nitramide

Basis Set	Geometry	Energy (Hartrees)[a]		ΔE
		Ground (C_s)	Transition (C_{2v})	(kcal/mol)
SCF/6-31G*	SCF/6-31G*	-260.321255	-260.316997	2.67
SCF/6-31G*	MP2/6-31G*	-259.628439	-259.626170	1.43
MP2/6-31G*	"	-260.329635	-260.324810	3.03
MP3/6-31G*	"	-260.317725	-260.313389	2.72
MP4D/6-31G*	"	-260.337230	-260.332097	3.22
MP4DQ/6-31G*	"	-260.322156	-260.317415	2.98
MP4SQD/6-31G*	"	-260.334381	-260.329332	3.17
CCSD/6-31G*	"	-260.331320	-260.326389	3.09
CCSD(T)/6-31G*	"	-260.357763	-260.352152	3.52
SCF/6-311G*	SCF/6-311G*	-260.455011	-260.449873	3.22
MP2/6-311G*	MP2/6-311G*	-260.461337	-260.455783	3.48
SCF/6-311G**	SCF/6-311G**	-260.471814	-260.466894	3.09
MP2/6-311G**	MP2/6-311G**	-260.478242	-260.472773	3.43
MP2/6-311+G**	MP2/6-311G**	-260.493288	-260.488302	3.13
MP2/6-311++G**	"	-260.493495	-260.488444	3.17
MP2/6-311G(2d,p)	"	-260.536130	-260.531518	2.89
MP2/6-311G(2df,p)	"	-260.614155	-260.610460	2.32
MP2/6-311G(3df,p)	"	-260.631814	-260.628083	2.34
MP2/6-311G(3d2f,p)	"	-260.644624	-260.641057	2.24
MP2/6-311G(2df,2p)	"	-260.618654	-260.614765	2.57
MP2/6-311+G(2df,2p)	"			
(SCF)	"	-259.738050	-259.736555	0.94
(MP2)	"	-260.632177	-260.628925	2.04
(MP3)	"	-260.614779	-260.611789	1.88
(MP4D)	"	-260.638018	-260.634308	2.33
(MP4DQ)	"	-260.614080	-260.610757	2.09
(MP4SDQ)	"	-260.629072	-260.625428	2.29
(CCSD)	"	-260.624553	-260.621039	2.21
(CCSD(T))	"	-260.667943	-260.663887	2.55
MP2/6-311+G(2df,3p)	"	-260.632552	-260.629273	2.06
Experiment[b]				2.7

[a] Single point energies at the level of theory in column 1 using geometries determined at the level of theory in column 2. [b]Fom ref. 13

Table 2

Optimized Geometry for Nitramide (C_s)

BASIS	6-31G*		6-311G*		6-311G**		Experiment	
LEVEL	SCF	MP2	SCF	MP2	SCF	MP2	Ref. 14[a]	Ref. 15[b]
Bond Lengths (Å)								
O-N	1.190	1.234	1.184	1.221	1.183	1.221	1.232	1.206
N-N	1.356	1.400	1.359	1.402	1.360	1.399	1.381	1.427
N-H	1.000	1.017	0.997	1.013	0.995	1.011	1.007	1.005
Valence Angles (degrees)								
O-N-O	127.0	127.7	127.0	127.8	127.0	127.7	132.7	130.1
O-N-N	116.5	116.1	116.5	116.1	116.5	116.1		
H-N-N	110.5	108.3	110.6	108.2	110.4	108.5		
H-N-H	116.8	114.6	116.8	114.0	115.9	114.5	120.9	115.2
Dihedrals and Out-of-Plane Angles (degrees)								
H N N O	-156.4	-154.1	-156.6	-153.8	-155.9	-154.4	-157.1	-154.2
O-N-N*-O	177.7	176.2	177.4	175.9	177.3	175.8	177.6	175.6
∠ (HNH) (ONO)[c]	46.0	51.0	45.6	51.3	46.6	50.2	46.9	51.8

[a] Gas phase microwave spectroscopy data. [b] Gas phase electron diffraction data. [c] Angle between the planes containing HNH and ONO atom centers.

Table 3

Geometries of Dimethylnitramine

	Ground state (C_s)			Saddle Point (C_{2V})			Experiment	
	SCF	MP2	F.F.[a]	SCF	MP2	F.F.	Ref. 17[b]	Ref. 18[c]
				Bond lengths (Å)				
O-N	1.190	1.227	1.233	1.194	1.232	1.232	1.223	1.240
N-N	1.349	1.396	1.408	1.327	1.363	1.404	1.382	1.334
C-N	1.456	1.459	1.461	1.453	1.450	1.459	1.46	1.458
<C-H>	1.081	1.092	1.090	1.081	1.092	1.091	1.121	
				Valence Angles				
O-N-O	125.15	126.2	125.2	125.3	126.5	125.8	130.4	124.3
O-N-N	117.4	116.9	117.4	117.4	116.7	117.1		
C-N-N	115.7	113.3	113.7	117.7	117.0	117.6		
C-N-C	119.3	116.6	117.7	124.9	126.0	124.8	127.6	124.7
<N-C-H>	109.7	110.0	109.7	109.8	109.7	109.6		
				Dihedral and Out-of-plane Angles				
O-N-O-*N	1.8	3.1	0.4	0.0	0.0	0.0		
C-N-N-O	-164.0	-159.3	-159.2	180.0	180.0	180.0		
N-N-C-H	65.4	62.6	61.9	60.7	60.3	60.2		
∠(CNC) (N-N)[d]	31.1	41.3	39.3	0.0	0.0	0.0	0.0	0.0
∠(CNC) (ONO)[e]	29.5	38.4		0.0	0.0		0.0	0.0

[a] F.F. = force field value. [b]Gas phase electron diffraction data. [c]X-ray diffraction data. [d]Angle between the plane containing the CNC atoms and the N-N bond vector. [e]Angle between the planes containing the CNC and ONO atom centers.

Table 4

Force Field Parameters for DMNA

Bond Stretches, $U = \frac{1}{2} k^s_{ij} (r_{ij} - r^o_{ij})^2$

Stretch	k^s_{ij} (kcal mol^{-1} Å^{-2})	r^o_{ij} (Å)
O-N	1990.1	1.23
N-N	991.7	1.36
N-C	672.1	1.44
C-H	641.6	1.09

Valence Bends, $U = \frac{1}{2} k^b_{ijk} (\theta_{ijk} - \theta^o_{ijk})^2$

Bend	k^b_{ijk} (kcal mol^{-1} rad^{-2})	θ^o_{ijk} (rad)
O-N-O	125.0	2.1104
O-N-N	125.0	1.8754
N-N-C	130.0	1.6723
C-N-C	70.0	1.8430
N-C-H	86.4	1.8676
H-C-H	77.0	1.8938

Torsions, $U = \frac{1}{2} k^t_{ijkl} [1 - \cos(n\phi_{ijkl})]$

Torsion	k^t_{ijkl} (kcal mol^{-1})	n
O-N-N-C	8.45	2
O-N-N-C	0.79	4
O-N-N-C	0.004	8
H-C-N-N	-0.16	3

Out-of-plane bends, $U = \frac{1}{2} k^d_{ijkl} \delta_{ijkl}^2$

Out-of-plane bend	k^d_{ijkl} (kcal mol^{-1} rad^{-2})
*O-N-O-*N*	89.3

Nonbonded, $U = A_{ij} \exp(- B_{ij} r_{ij}) - C_{ij} / r_{ij}^6$

Atoms	A_{ij} (kcal mol^{-1})	B_{ij} (Å^{-1})	C_{ij} (kcal mol^{-1} Å^6)
C···C	14976.0	3.090	640.8
H···H	2649.7	3.740	27.4
C···H	4320.0	3.415	138.2
N···N	60833.9	3.780	500.0
O···O	75844.8	4.063	398.9

Electrostatic, $U = q_i q_j / r_{ij}$

Atom Type	q_i (esu)
C	-0.49445
H	0.18939
N (nitro)	0.67253
N (amine)	-0.06836
O	-0.37576

Table 5

Correlation times and Activation Energies for Molecular Reorientation

Parameter	Experiment[a]	Experiment[b]	MD[c] (t_{kww})	MD[d] (t_c)
Activation Energy (kcal/mol)	2.7	2.4	2.61	2.63
Correlation time at 298K, t (ps)	2.6	1.9	3.47	4.24

[a] DMNA in Tetrachloroethylene (Ref. 20). [b] DMNA in Pyridine (Ref. 20). [c] from equation 5, based on linear extrapolation of MD data to 298 K. [d] from equation 6, based on linear extrapolation of MD data to 298 K.

Figure Captions

Figure 1. Representation of the C_s-ground, C_{2v}-saddle (inversion) and the C_s-saddle (rotation) states of nitramide (*a*, *b*, *c*) and dimethylnitramine (*d*, *e*, *f*). The white circles represent carbon, solid black circles represent oxygen, patterned gray represents nitrogen and solid gray represent hydrogen atoms.

Figure 2. The conformational energy of DMNA as a function of the O-N-N-C dihedral angle as determined from quantum chemistry and the quantum chemistry based force field.

Figure 3. The gas-phase radial distribution function for DMNA as obtained from electron diffraction (343 K) and Brownian dynamics simulation (350 K).

Figure 4. The inversion potential for gas and liquid-phase DMNA at 350 K. Gas and liquid phase simulations were performed using Brownian and molecular dynamics respectively. The out of plane angle is defined as the angle between the N-N bond and the C-N-C plane. Also shown are results from quantum chemistry calculations.

Figure 5. (a) Specific volume vs. temperature for liquid DMNA at 1 atm from molecular dynamics simulations. The experimental point at 345 K is from ref. 30. (b) The pressure-volume isotherm for liquid DMNA at 350 K from molecular dynamics simulations. The MD points have been fit with a second order polynomial curve (solid line). Error bars indicating 95% confidence levels are either shown or are smaller than the plot symbols.

Figure 6. Temperature dependence of the solubility parameter of liquid DMNA from MD simulation. The broken line is a second order polynomial fit to the MD

data. The open circle is from experiment. Error bars indicating 95% confidence levels are shown.

Figure 7. Temperature dependence of the inversion rate (at the amine nitrogen) in liquid DMNA. The activation energy for the process is also shown. Error bars indicating 95% confidence levels are shown. The error bars correspond to approximately 3 % of the mean inversion rate values.

Figure 8. First (P_1) and second (P_2) order orientational autocorrelation functions for liquid DMNA. The MD points have been fit by a stretched exponential (eq. 5).

Figure 9. Temperature dependence of the relaxation and correlation time (t) associated with the decay of P_1 and P_2 orientational autocorrelation functions. Error bars indicating 95% confidence levels are shown. The error bars correspond to approximately 10 % of the mean t values.

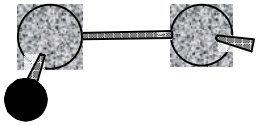

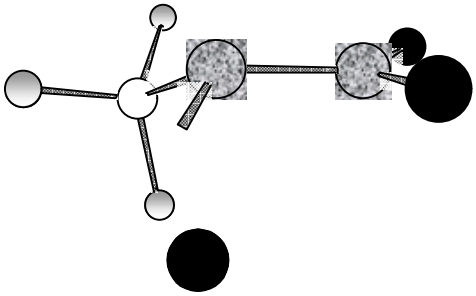

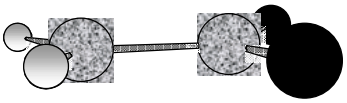

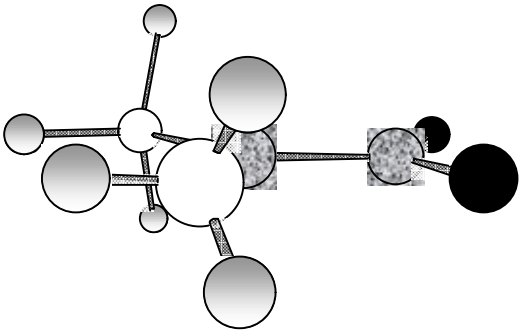

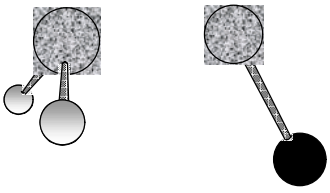

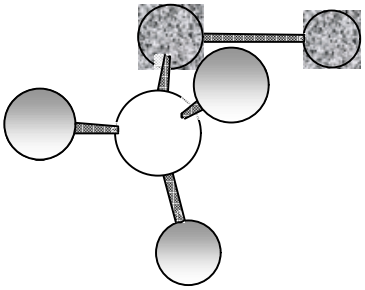

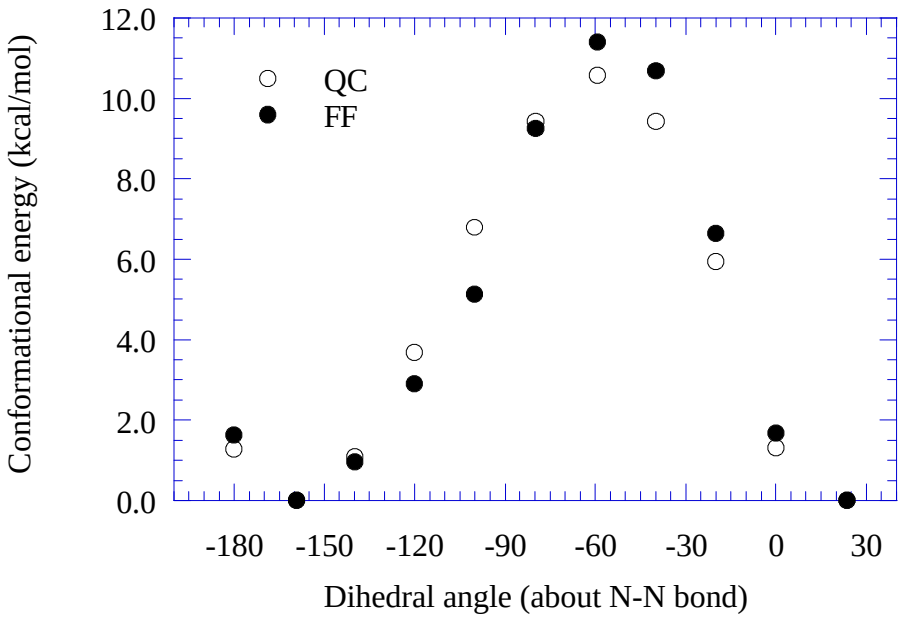
12.0
10.0
8.0
6.0
4.0
2.0
0.0
Conformational energy (kcal/mol)
QC
FF
-180
-150
-120
-90
-60
-30
0
30
Dihedral angle (about N-N bond)

Figure 2

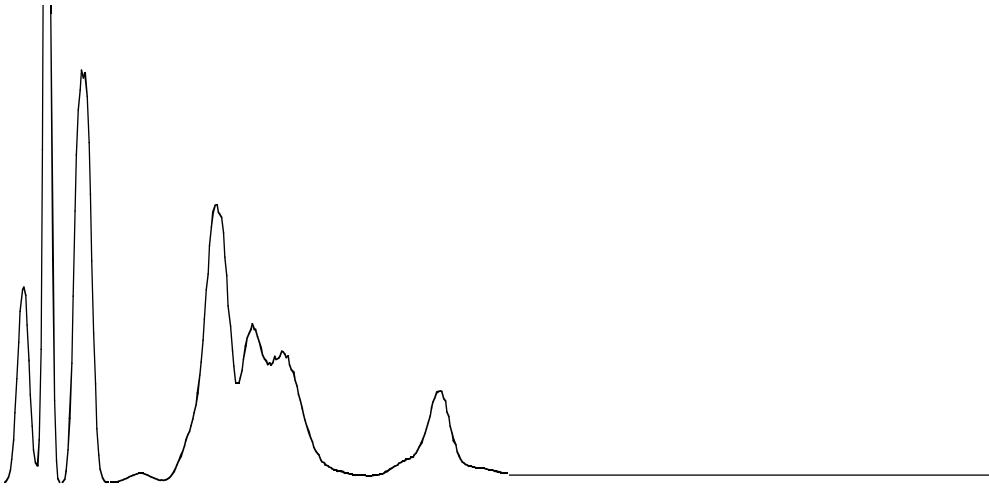

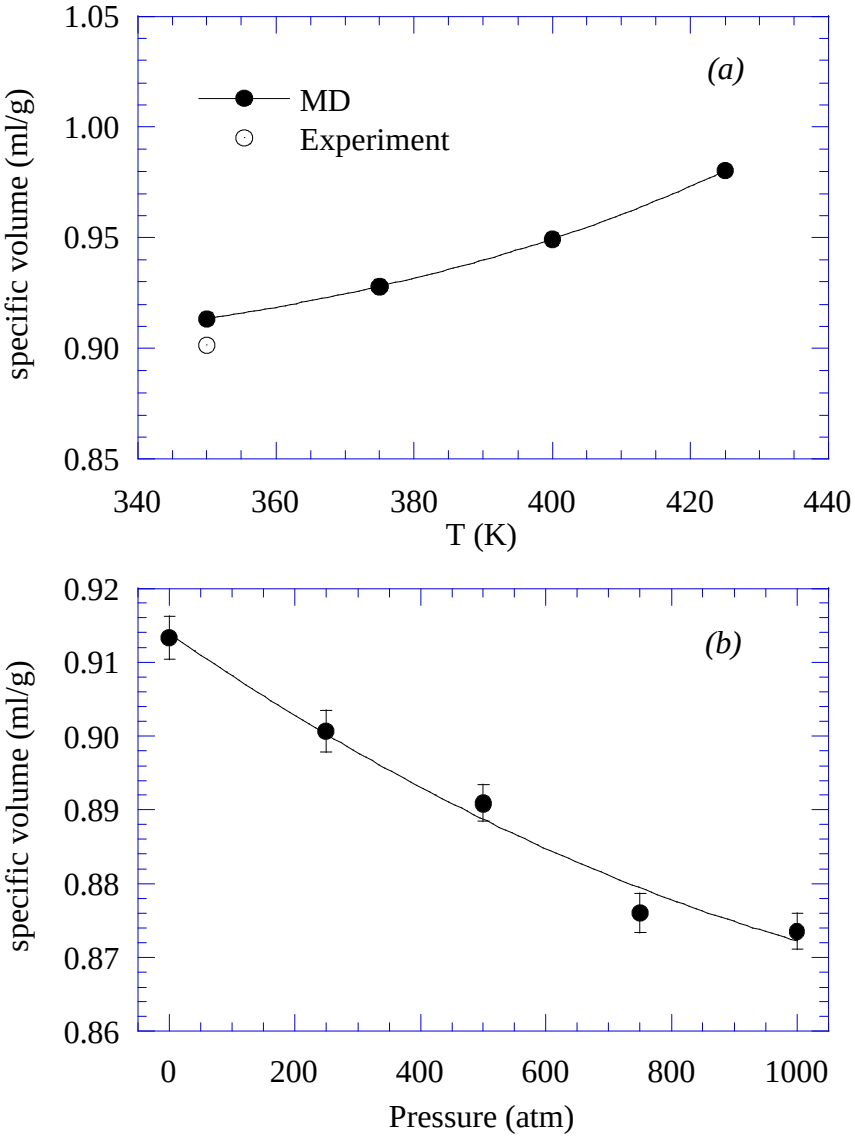
1.05
1.00
0.95
0.90
0.85
specific volume (ml/g)
(a)
MD
Experiment
340
360
380
400
420
440
T (K)
0.92
0.91
0.90
0.89
0.88
0.87
0.86
specific volume (ml/g)
(b)
0
200
400
600
800
1000
Pressure (atm)

Figure 5

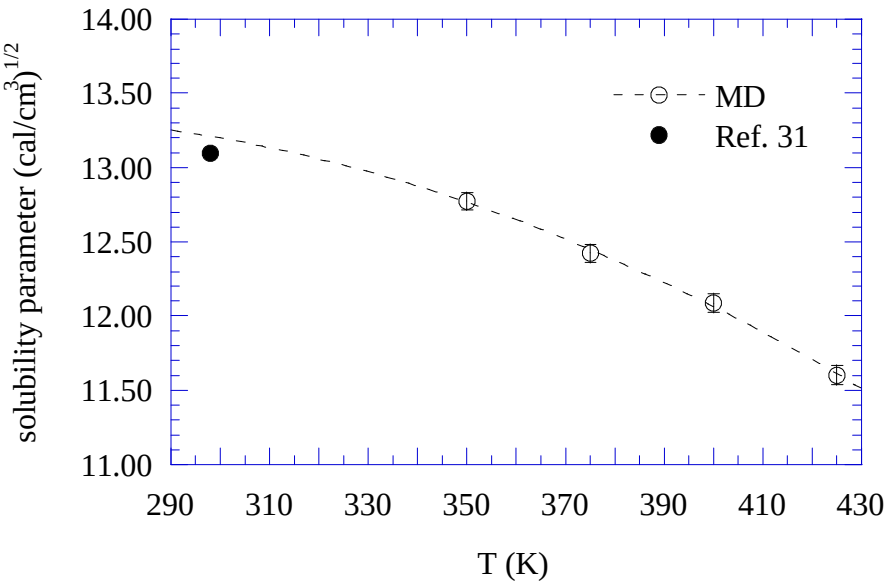
14.00
13.50
13.00
12.50
12.00
11.50
11.00
290
310
330
350
370
390
410
430
T (K)
solubility parameter (cal/cm3)1/2
MD
Ref. 31

Figure 6

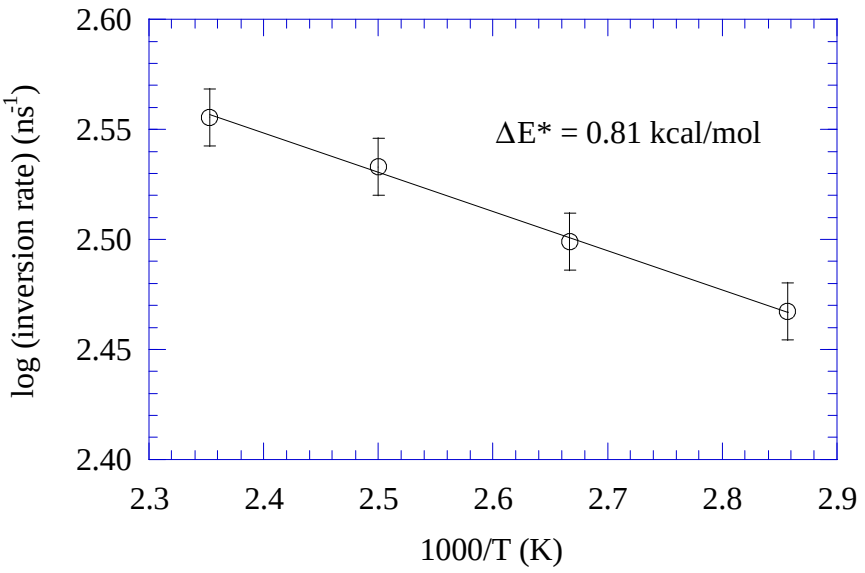
2.60
2.55
2.50
2.45
2.40
log (inversion rate) (ns-1)
ΔE* = 0.81 kcal/mol
2.3
2.4
2.5
2.6
2.7
2.8
2.9
1000/T (K)

Figure 7

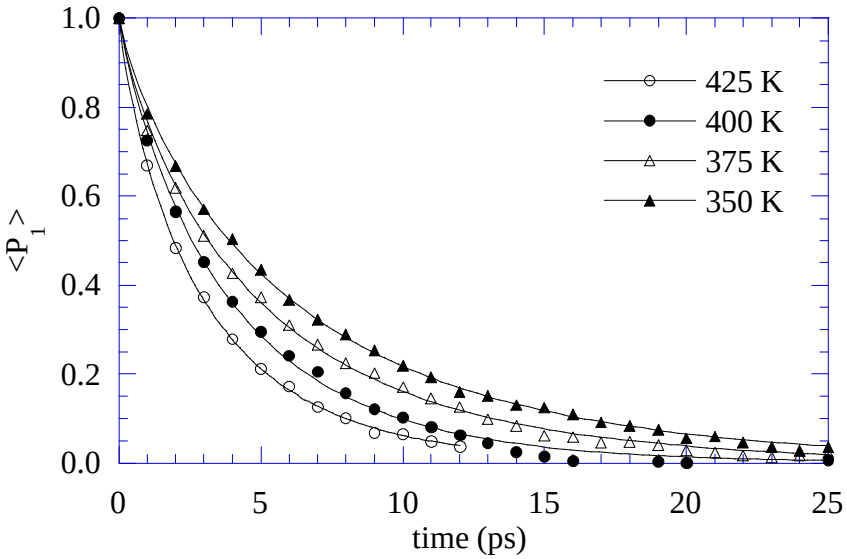
1.0
0.8
0.6
0.4
0.2
0.0
<P1>
0
5
10
15
20
25
time (ps)
425 K
400 K
375 K
350 K

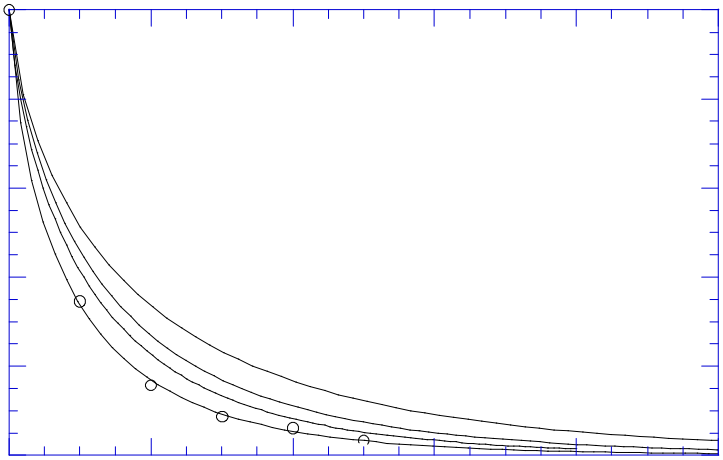

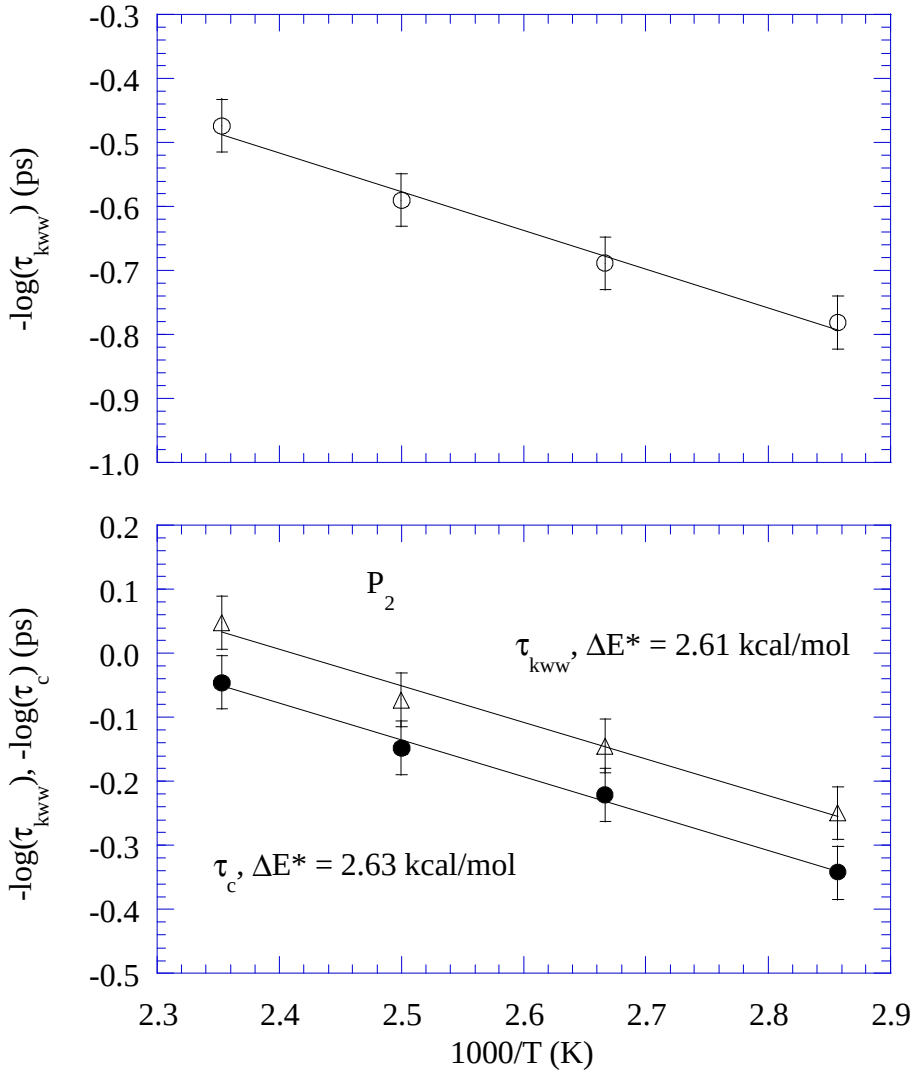
-0.3
-0.4
-0.5
-0.6
-0.7
-0.8
-0.9
-1.0
-log(τkww) (ps)
0.2
0.1
0.0
-0.1
-0.2
-0.3
-0.4
-0.5
-log(τkww), -log(τc) (ps)
P2
τkww, ΔE* = 2.61 kcal/mol
τc, ΔE* = 2.63 kcal/mol
2.3
2.4
2.5
2.6
2.7
2.8
2.9
1000/T (K)

References

(1) (a) Jaffe, R. L.; Smith, G. D.; Yoon, D. Y. *J. Phys. Chem.* **1993**, *97*, 12745. (b) Smith, G. D.; Jaffe, R. L.; Yoon, D. Y. *J. Phys. Chem.* **1993**, *97*, 12752. (c) Smith, G. D.; Jaffe, R. L.; Yoon, D. Y. *J. Am. Chem. Soc.* **1995**, *117*, 530.

(2) Smith, G. D.; Borodin, O.; Pekny, M.; Annis, B.; Londono, D.; Jaffe, R. L. *Spectochimica Acta A* **1997**, *53*, 1273.

(3) Sorescu, D. C.; Rice, B. M.; Thompson, D. L. *J. Phys. Chem. B* **1997**, *101*, 798.

(4) (a) Sewell, T. D. *J. Appl. Phys.* **1998**, *83*, 4142. (b) Sewell, T. D. in "Shock Compression of Condensed Matter," Schmidt, S. ed., Proc. of 1997 American Physical Society Topical Conference on Shock Compression of Condensed Matter, University of Massachussetts, Amherst, MA., July 27- August 1, 1997.

(5) Ritchie, J. P. *J. Am. Chem. Soc.* **1989**, *111*, 2517.

(6) Sumpter, B. G.; Thompson, D. L. *J. Chem. Phys.* **1988**, *88*, 6889

(7) (a) Politzer, P.; Sukumar, N.; Jayasuriya, K.; Ranganathan, S. *J. Am. Chem. Soc.* **1988**, *110*, 3425. (b) Habibollahzadeh, D.; Murray, J. S.; Redfern, P. C.; Politzer, P. *J. Phys. Chem.* **1991**, *95*, 7703.

(8) Kohno, Y.; Maekawa, K.; Tsuchioka, T.; Hashizume, T.; Imamura, A. *Chem. Phys. Lett.* **1993**, *214*, 603

(9) Roszak, S. *J. Mol Struct.* **1994**, *304*, 269.

(10) (a) Khaikin, L. S.; Grikina, O. E.; Vilkov, L. V.; Palafox, A. M.; Boggs, J.E. *J. Struct. Chem.* **1993**, 34, 2. (b) Khaikin, L. S.; Grikina, O. E.; Vilkov, L. V.; Boggs, J. E. *J. Struct. Chem.* **1993**, *34*, 9.

(11) Harris, J. N.; Lammertsma, K. *J. Phys. Chem. A* 1997, 101, 1370.

(12) Frisch, M. J.; Trucks, G. W.; Schlegel, H. B.; W. Gill, P. M.; Johnson, B. G.; Robb, M. A.; Cheeseman, J. R.; Keith, T.; Petersson, G. A.; Montgomery, J. A.; Raghavachari, K.; Al-Laham, M. A.; Zakrzewski, V. G.; Ortiz, J. V.; Foresman, J. B.; Cioslowski, J.; Stefanov, B. B.; Nanayakkara, A.; Challacombe, M.; Peng, C. Y.; Ayala, P. Y.; Chen, W.; Wong, M. W.; Andres, J. L.; Replogle, E. S.; Gomperts, R.; Martin, R. L.; Fox, D. J.; Binkley, J. S.; Defrees, D. J.; Baker, J.; Stewart, J. P.; Head-Gordon, M.; Gonzalez, C.; Pople, J. A. *Gaussian 94*, Gaussian, Inc.: Pittsburgh PA, 1995.

(13) Lister, D. G.; Tyler, J. K. *Chem. Comm*. **1966**, 152.

(14) Tyler, J. K. *J. Mol. Spectrosc.* **1963**, *11*, 39.

(15) Sadova, N. I.; Slepnev, G. E.; Tarasenko, N. A.; Zenkin, A. A.; Vilkov, L. V.; Shishkov, I. F.; Pankrushev, Y. A. *Zh. Strukt. Khim.* **1977**, *18*, 865.

(16) Hunter, E. C.; Partington, J. R. *J. Chem. Soc.* **1933**, 309.

(17) Stolevik, R.; Rademacher, P. *Acta. Chem. Scand*. **1969**, *23*, 672.

(18) Krebs, B.; Mandt, J. *Acta. Cryst.* **1979**, *B35*, 402.

(19) Filhol, A.; Bravic, G.; Rey-Lafon, M.; Thomas, M. *Acta. Cryst.* **1980**, *B36*, 575.

(20) Kitzinger, J. P.; Lehn, J. M.; Williams, R. L. *Mol. Phys.* **1969**, *17*, 135.

(21) Swalen, J. D.; Ibers, J. A. *J. Chem. Phys.* **1962**, *36*, 1914.

(22) Tsuboi, M,; Hirakawa, A. Y.; Tamagake, K. *J. Mol. Spectrosc*. **1967**, *22*, 272.

(23) The MOLBD3 force field is available in the POLYMER module of the SYBYL simulation software of the Tripos Co., St. Louis MO.

(24) Sorensen, R. A.; Liau, W. B.; Kesner, K.; Boyd. R. H. *Macromolecules* **1988**, *21*, 200.

(25) Smith, G. D. in "Computational Materials research," Hinkley, J.A. and Gates, T. S. ed., NASA Conference Publication 10190, Williamsburg, Virginia, January 4-5, 1996.

(26) Van Gunsteren, W. F.; Berendsen, J. C. H. *Mol. Phys.* **1982**, *45*, 637.

(27) (a) Rymer, T. B. *Electron diffraction*, Methuen, London, 1970. (b) Hargittai, I. In *Stereochemical Applications of Gas Phase Electron Diffraction*, Part A, Hargittai, I.; Hargittai, M., Eds.; VCH Press: New York, 1988.

(28) (a) Andersen, H. C. *J. Chem. Phys*. **1980**, *72*, 2384. (b) Nose, S. *J. Chem. Phys*. **1984**, *81*,511. (c) Hoover, W. G. *Phys. Rev. A* **1985**, *31*, 1695.

(29) Martyna, G. J.; Tuckerman, M. E.; Tobias, D. J.; Klien, M. L. *Mol. Phys*. **1996**, *87*, 1117.

(30) *CRC Handbook of Chemistry and Physics*; Lide, D. R., Ed.; CRC Press: Boca Raton, Fl, 1998.

(31) Brandrup, J.; Immergut, E. H. *Polymer Handbook*, 3rd ed.; Wiley-Interscience: New York, 1989.